Angkasa Jurnal Ilmiah Bidang Teknologi
ISSN : 2085-9503 (Print)
ISSN : 2581-1355 (On Line)
Accredited Fourth Grade by Kemenristekdikti, Decree No: 148/M/KPT/2020
DOI : 10.28989/ angkasa.v14i1.1170

Numerical study of drag force on the UAV tilt and fixed wing model during vertical take off landing

Muhammad Musyfiq Haikal[1], Rully Hidayat[2], Bahrul Jalaali[*,3]
[1,2,3] Department of Mechanical Engineering, Adisutjipto Aerospace Institute of Technology

Article Info

Article history:

Received January 5, 2022
Accepted February 2, 2022
Published May 1, 2022

Keywords:

Computational Fluid dynamics
UAV Aircraft
Drag
VTOL

ABSTRACT

A hybrid vertical take-off landing (VTOL) UAV combines the concepts of fixed-wing and rotary-wing UAV aircraft in one platform while performing in both conventional and vertical take-off landings. This aircraft has a drawback of significant drag force generated due to fixed-wing. Therefore, a Tilt-Wing often utilized to overcome this obstacle whereby it could be adjusted to the vertical and horizontal directions. To enhance the understanding of generated drag force on both wing model, this study was performed by examine the drag characteristic of the VTOL UAV. The simulations were carried out in the wind speed range by 1.4 m/s, 4.17 m/s, and 6.94 m/s. Simulation results showed that the drag of the UAV Hybrid Tilt-Wing and Fixed-Wing increased at the speed of 1.4 m/s to 6.94 m/s while the highest drag value was 177.51 N on a Fixed-Wing UAV aircraft and 1.97 N on a Tilt-Wing UAV aircraft. The result concluded that Tilt-Wing UAV has less drag which was more efficient than fixed-wing.

Corresponding Author:

Bahrul Jalaali,
Department of Mechanical Engineering,
Adisutjipto Aerospace Institute of Technology
Jl. Majapahit Blok - R Lanud Adisutjipto Yogyakarta
Email: *bahrul@itda.ac.id

1. INTRODUCTION

UAV (Unmanned Aerial Vehicle) aircrafts are often used, for instances: rural firefighting and rescue mission. However, it currently is still challenging to develop a small-scale UAV which is capable to achieve long flight endurance and range. In addition, it is also beneficial for the UAV that can control vertical take-off and land simultaneously. The Hybrid vertical take-off landing (VTOL) UAV combines the concepts of fixed-wing UAV aircraft and rotary-wing UAV aircraft in one platform. It has advantage on the vertical take-off and landing. Hence, it will be advantageous for such a UAV with a VTOL scheme. Unfortunately, the relatively high drag that occurred in VTOL becomes the obstacle that reduced the performance of flight endurance and range.

In general, the drag analysis can be performed in the scope of three methods, i.e., analytical solution, experimental, and numerical approximation. It is noteworthy analytical solutions are mainly beneficial when solving specific basic and straightforward problems. The experimental is, however, often costly and burdensome to be conducted [1]. Furthermore, experiments may not provide the sets of data needed for achieving a reliable design. [2]. Several efforts have been made to find a suitable model to investigate the

aerodynamics characteristics. Previously, both experimental and numerical studies had been performed accordingly. Aerodynamics assessment on an airfoil was performed by a practical test as reported in Refs. [3-7]. The studies found that the airfoil flow characteristic was typically obtained as pressure and velocity distribution and lift-drag characteristics. Rao et al. [8] and Li et al. [4] found that the lift-to-drag coefficient was related to the flap addition. A similar trend was also found by Rhee et al. [5] towards hydrofoil, Roztamzadeh et al. [7] on the undulated airfoil, and Kulshrestha et al. [9] on the NACA airfoil solved using Finite Element Method (FEM). Meanwhile, a study of VTOL was performed by Cronin [10]. It revealed that the FWD rotor affects the incoming airflow and causes downwash on the wing leads to the impacts of lift generation by the wing. The study of Kurniawan [11] stated that the distribution of fluid flow arising from Airflow rate was directly proportional to velocity. However, only slight studies revealed the drag characteristic on the VTOL UAV to the best author known. Therefore, this study is proposed to give deeper observation on drag characteristic through numerical model.

Furthermore, to accurately examine the numerical result, studies of the turbulence model have been conducted. The comparison between CFD and experimental results showed significant discrepancies due to the turbulent model selection [2]. In other studies, the k-ω turbulence model had also been used and shown a significant deviation from the experimental [5]. On Refs. [12,14-16], explicit modeling approaches were used for the laminar-turbulent transition. The transitional model coupled with the k-ω turbulence model yielded a problem in the transition of laminar-turbulence at a high angle of attack (α) [17]. However, the causes had not been detailed explained. The turbulence model of k-ε and k-ω calculate variables of turbulence kinetic energy and the rate of turbulence kinetic energy dissipation. Those models have disadvantages in flow fields that exhibit adverse pressure gradients while performed well on the internal flow [18]. On the other hand, the Spalart-Allmaras (S-A) equation-based model for transitional flows has been widely used for aerospace applications, as reported by Refs. [19,20]. The model was reliable on several aerodynamic characteristics and exhibited stable and good numerical convergence [18]. The S-A model calculates a transport equation for kinematic viscosity, while it does not consider the calculation of length scale related to the shear layer thickness. Therefore, this study utilized the S-A to investigate the aerodynamic characteristics.

A brief description of this work is given in the following points. First, this study aims to simulate the VTOL UAV using CFD approximation to investigate the behavior of aerodynamic characteristics. The study also profoundly investigates the aspect of Tilt-Wing UAVs. Second, the analysis of drag reduction is performed by varying the wind velocity at the inlet. The developed model's implementation is also intended to be a general model in VTOL UAV simulation to obtain the optimum design. The rest of the paper is organized as follows: The geometry, numerical setup, and theoretical consideration are presented in Section 2. Section 3 gives the numerical result while the findings and conclusions are then listed in Section 4.

2. METHODS

In the present work, the simplified step of the simulation process shows in flowchart Figure 1. The problem formulation of this work is the investigation of drag force towards tilt and fixed UAV wing. The CFD study can be approximate as a wind tunnel where the geometry is examined within the particular domain [1]. Hence, it needs to model the geometry and surrounding airflow to conduct the fluid dynamics analysis. In the progressive work, we will profoundly discuss the steps of simulation. The validation towards NASA Technical Memorandum 4074 experimental result was conducted to ensure the accurate result.

 ISSN : 2085-9503 (Print), 2581-1355 (On Line)

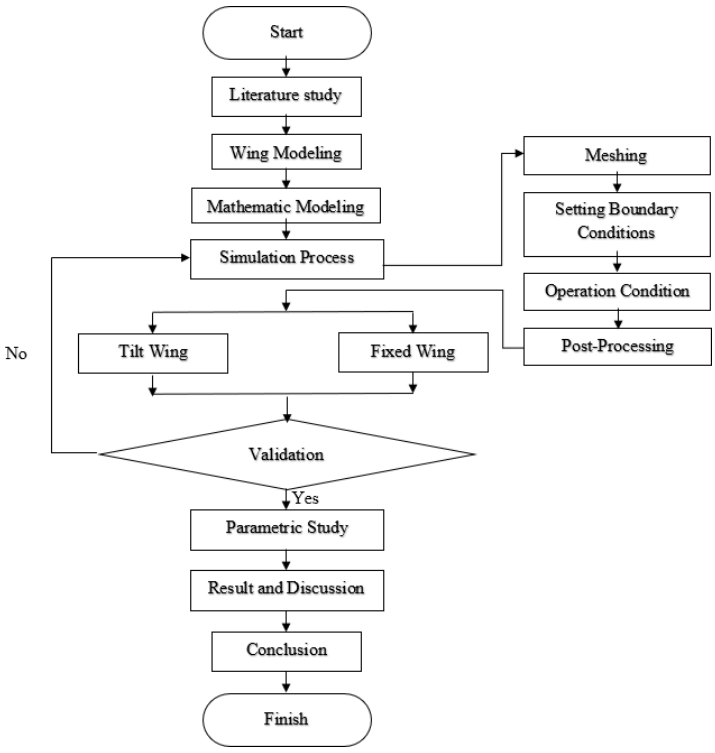

Figure 1. Flowchart for simulation process

The wing based on NACA 0012 airfoil was utilized while the wing models are divided into two categories: Tilt-Wing (vertical) and Fixed-Wing (horizontal). The designs are shown in Figures 2(a) and 2(b) whereby the design based on the previous literatures of [18]. The design was designed to observe both vertical and horizontal characteristics of drag. Here, it will be varied with some predefined parameters [13]. The specifications and the UAV model are listed in Table 1.

Table 1. UAV Aircraft Specifications

Parameter	Value	Unit
Fuselage Length	1.32	m
Wing Span Length	1.71	m
Wing Chord Length	0.25	m
Wing Area	0.42	m^2
Aspect Ratio	7	
Tail Moment Arm	0.86	m
Horizontal Stabilizer Area	0.06	m^2
Vertical Stabilizer Area	0.03	m^2
Span Vertical Stabilizer Length	0.23	m
Tapper Ratio	0.45	
Aspect Ratio	1.65	

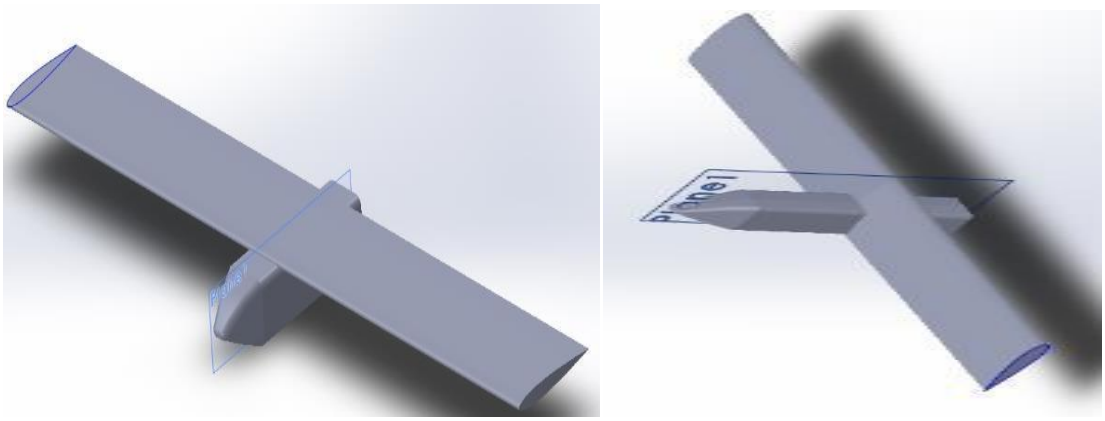

(a) (b)

Figure 1. UAV model of (a) Fixed-Wing (b) Tilt-Wing

The mathematical formulation of the fluid analysis is carried out by using governing equations of mass and transport. The governing equations used in this model are presented in terms of continuity equation (Eq 1) for mass balance. Navier-Stokes equation (Eq. 2) to represent the momentum balance. and Spalart Allmaras (S-A) for analyzing the turbulence model (Eq. 3). The nomenclatures are stated in Table 2. This step was done by determining the simulation parameters. such as; the airflow velocity. solid surface geometry. wall function. drag force and flow regime. Those equations represent 5 transport equations in 7 unknow variable i.e: $u.\ v.\ w.\ p.\ T.\ \rho.\ \tilde{\upsilon}$. In this work. we employ the standard model of S-A turbulent presented in both Refs [18] and [19]. Furthermore, the production and destruction of turbulent viscosity in the near-wall region are stated in Eqs. 4 and 5. The variable considered is S-A model is the turbulent viscosity ($\tilde{\upsilon}$). It is in accordance in the regions which are not affected by a strong viscous effect. The transport equation of S-A consists of production. source and destruction term.

$$\frac{D\rho}{Dt} + \rho\nabla.\vec{\boldsymbol{V}} = 0 \tag{1}$$

$$\rho\left(\frac{\partial \boldsymbol{V}}{\partial t} + \boldsymbol{V}.\nabla\mathbf{V}\right) = \nabla\boldsymbol{P} + \rho\boldsymbol{g} + \mu\nabla^2\boldsymbol{V} \tag{2}$$

$$\frac{D\tilde{\upsilon}}{Dt} = G_\upsilon - Y_\upsilon + \frac{1}{\widetilde{\sigma_\upsilon}}[\nabla.\{(\upsilon + \tilde{\upsilon})\nabla\tilde{\upsilon}\} + C_{b2}(\nabla\tilde{\upsilon})^2] + S_{\tilde{\upsilon}} \tag{3}$$

Where:

$$G_\upsilon = C_{b1}\rho\left(S + \frac{\tilde{\upsilon}}{\kappa^2 d^3}\left(1 - \frac{\chi}{1+\chi f_{\upsilon 1}}\right)\right)\tilde{\upsilon}\ ;\ \chi = \frac{\tilde{\upsilon}}{\upsilon} \tag{4}$$

$$Y_\upsilon = \left(\frac{C_{b1}}{\kappa^2} + \frac{(1+C_{b2})}{\widetilde{\sigma_\upsilon}}\right)\rho g_t\left[\frac{1+{C_{w3}}^6}{{g_t}^6+{C_{w3}}^6}\right]^{\frac{1}{6}}\left(\frac{\tilde{\upsilon}}{d}\right)^2 \tag{5}$$

$$S = \sqrt{2(\frac{1}{2}(\frac{\partial \boldsymbol{u}_i}{\partial x_j} - \frac{\partial \boldsymbol{u}_j}{\partial x_i}))(\frac{1}{2}\left(\frac{\partial \boldsymbol{u}_i}{\partial x_j} - \frac{\partial \boldsymbol{u}_j}{\partial x_i}\right))} \tag{6}$$

$$g_t = \left(\zeta + C_{w2}(\zeta^6 - \zeta)\right) \tag{7}$$

$$\zeta = \tilde{\upsilon}/\left[\left(S + \frac{\tilde{\upsilon}}{\kappa^2 d^3}\left(1 - \frac{\chi}{1+\chi f_{\upsilon 1}}\right)\right)\kappa^2 d^2\right] \tag{8}$$

 ISSN : 2085-9503 (Print), 2581-1355 (On Line)

Table 2. Nomenclature

Symbol	Nomenclature	Unit
ρ	Density of fluid	kg/m^3
P	Pressure	Pa
g	Gravitational acceleration	m/s^2
μ	Dynamic viscosity	kg/m-s
V	Velocity vector	m/s
υ	Kinematic viscosity	m^2/s
$\tilde{\upsilon}$	Turbulent kinematic viscosity	m^2/s
S	Scalar measure of deformation tensor	m
d	Distance from the wall	m
S_υ	Source term	m^2/s
Y_υ	Destruction of turbulent viscosity	m^2/s
G_T	Production of turbulent viscosity	m^2/s
S	Magnitude of the vorticity	m^2/s

The discretization scheme is an element-based finite-volume method with second-order discretization in space and time. The first step on FVM discretization is to integrate the governing equation over the elements into which domain has been subdivided [20]. In this study, physical domain is divided into an unstructured-grid control volume dominated by triangular control volumes. Here, the simplified explanation of how FVM work is presented. The FV equation is described in Eq. 9.

$$\frac{d}{dt}\int_{\Omega_A} U\, dA + \int_{\partial\Omega_A} \boldsymbol{F}(U).\boldsymbol{n} ds = \int_{\Omega_A} S(U,t)\, dA \tag{9}$$

Where Ω_A and $\partial\Omega_A$ are the interior and control volume boundary, respectively. The cell average is defined in Eq. 10. Since, this method determines the control volume area, thus Eq. 9 becomes Eq. 11.

$$U_A = \frac{1}{A_A}\int_{\Omega_A} U\, dA \tag{10}$$

$$A_A \frac{dU_A}{dt} + \int_{\partial\Omega_A} \boldsymbol{F}(U).\boldsymbol{n} ds = \int_{\Omega_A} S(U,t)\, dA \tag{11}$$

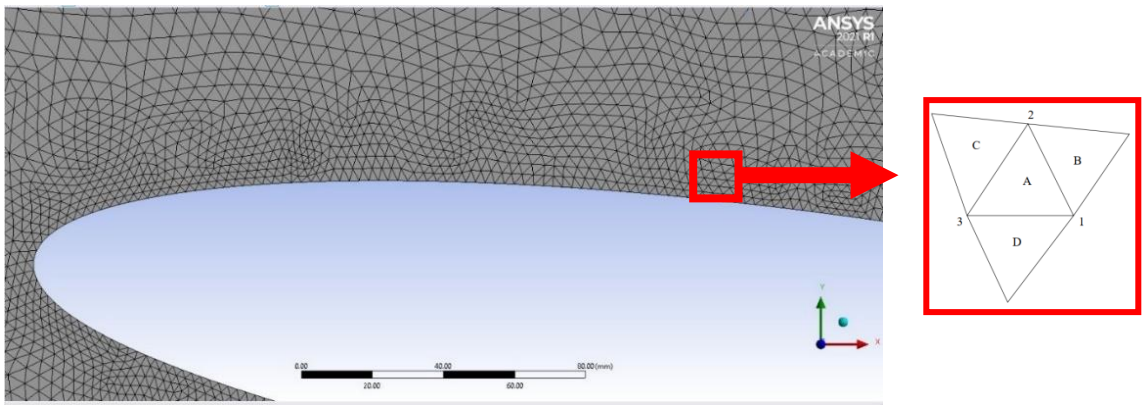

Figure 2. Simplified illustration of generated mesh

In case of discretization, S is assumed equals to 0. Hence, the surface integral for 3 edges in triangular domain declares as in Eq. 12. Whereby $H(U,\boldsymbol{n}) = \boldsymbol{F}(U).\boldsymbol{n}$ and $\boldsymbol{n}_{AB}$ is the unit of normal pointing from cell A to cell B (Fig. 2). The solution in control volume is equal to the cell average value as in one-dimensional case. The 'upwind' value using the velocity component normal to the face is used to determine the flux at

each interface (Eq. 13). The integration in the final step is performed using the forward Euler algorithm, resulting in the discrete FVM as stated in Eq. 14. The discretization step is applied to solve the governing equation.

$$A_A \frac{dU_A}{dt} + \int_1^2 H(U, \boldsymbol{n}_{AB})ds + \int_3^3 H(U, \boldsymbol{n}_{AC})ds + \int_3^1 H(U, \boldsymbol{n}_{AD})ds = 0 \quad (12)$$

$$H(U, \boldsymbol{n}_{AB}) \approx \widehat{H}(U_A, U_B, \boldsymbol{n}_{AB}) = \frac{1}{2}\boldsymbol{v}_{AB}.\boldsymbol{n}_{AB}(U_A + U_B) - \frac{1}{2}|\boldsymbol{v}_{AB}.\boldsymbol{n}_{AB}|\,(U_B - U_A) \quad (13)$$

$$A_A \frac{{U_A}^{n+1} - {U_A}^n}{\Delta t} + \widehat{H}({U_A}^n, {U_B}^n, \boldsymbol{n}_{AB})\Delta s_{AB} + \widehat{H}({U_A}^n, {U_C}^n, \boldsymbol{n}_{AC})\Delta s_{AC} + \widehat{H}({U_A}^n, {U_D}^n, \boldsymbol{n}_{AD})\Delta s_{AD} = 0 \quad (15)$$

A numerical study was done using commercial CFD of ANSYS. The initial and boundary condition are listed in Table 3. In the solver step, boundary conditions and input parameters were defined. Numerical modeling was carried out using a three-dimensional (3D) domain with full-scale dimensions. The viscous S-A model was chosen with vorticity-based and curvature correction addition, and the value of correction remains constant by 1. Some assumptions were made as an initial condition: fluid as an ideal gas, no heat transfer process, and the airflow determined at the subsonic domain. This, therefore, the pressure-based solver for the incompressible model was utilized. The no-slip wall boundary condition was applied at the surface of the airfoil. At the inlet, the turbulence properties were set to a turbulence intensity of 5% by using "medium intensity and Eddy viscosity ratio," and the zero pressure and uniform velocity were set. The fixed pressure value and zero velocity gradient were chosen at the outlet, and open boundary conditions were applied to the top and bottom of the wall domain. A high-resolution discretization scheme was used, and the calculation was performed on the constant initial and boundary conditions.

Table 3. Initial and boundary condition for the simulation

Parameter	Value	Unit
Type of analysis	Pressure-based, steady state	-
Residual	1 x 10^{-4}	-
Conservation target	1 x 10^{-5}	-
Turbulence numerics	First order	-
Air Density	1.2	kg/m^3
Inlet velocity	1.4, 4.17, 6.94	m/s
Outlet Pressure	0	Pa
Kinematic viscosity	1.8 x 10^{-5}	m^2/s
Dynamics viscosity	1.5 x 10^{-5}	kg/m-s
Temperature (*T*)	300	K
Gravity acceleration	9.81	m/s^2

3. RESULT AND DISCUSSION

3.1. Grid Study

Initially, the grid study was carried out in the simulation process to ensure no changes as the increase of grid number. In this study, the validation of the result was conducted by comparing the current results with NASA Technical Memorandum 4074 of NACA 0012. The coarse, medium and fine grids were generated. It was obtained that the optimum result on the fine grid (265mm face sizing), which provided less error. Hence, the same setup was used in the remaining setup of this study.

3.2. Simulation Result

The simulations have been conducted while the variation of parametric studies elaborated in Table 4. From Figure 3, it can be seen that the value of a drag UAV aircraft Hybrid Fixed-Wing increases with the increase of velocity. The lowest drag force was 7.69 N for A. Meanwhile, the drag force rose at about 88% at 64.6N for B variation, while the most prominent value was obtained at C by 177.51N. The qualitative results were also described in the same patterns as can be seen in Figures 4, 5, and 6 for pressure contour and streamlines. The flow around the wing tends to be more fluctuate, which leads to higher eddy at the high velocity. This caused more turbulence generated, which affected the drag.

Table 4. Notation of parametric studies

Notation	Value (m/s)
A	1.4
B	4.17

 ISSN : 2085-9503 (Print), 2581-1355 (On Line)

C	6.94

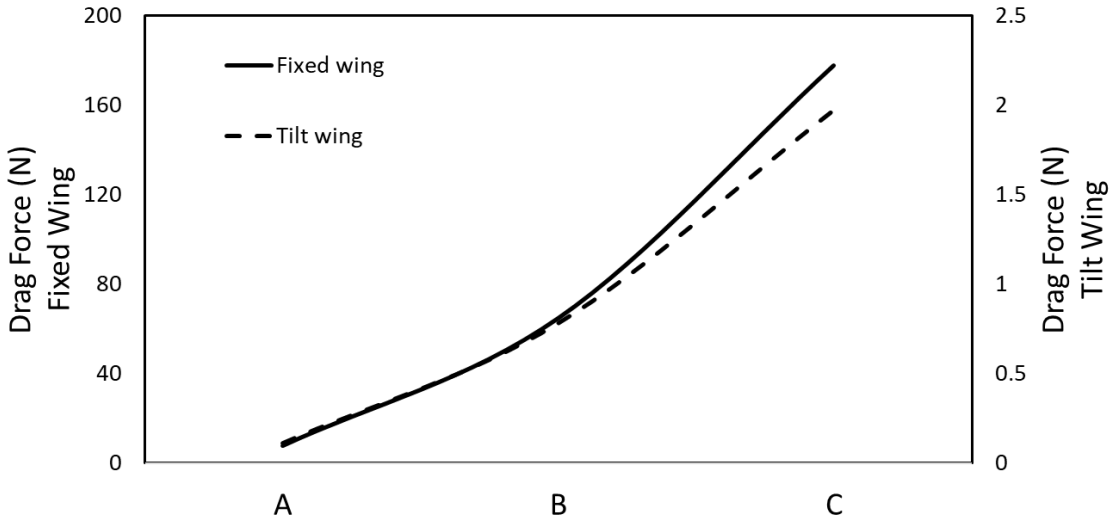

Figure 3. Drag force value of fixed and Tilt-Wing

The exact manner found on the value of drag the UAV Hybrid Tilt-Wing whereby it increased as well with the value of velocity. It was obtained that the lowest drag force was 0.11N at A while the highest was in C by 1.97 N. Those aforementioned values were considerably nearly less than tenfold than that of Fixed-Wing. Besides, Figures 4, 5, and 6 showed that the airflow at the adjacent wing's wall was observed far more stable than Fixed-Wing. This was the reason why the drag force was significantly small. This proves that drag force was influenced by velocity and wing orientation. It is also worth noting that the appearance of eddy leads to turbulent flow, which affects the drag.

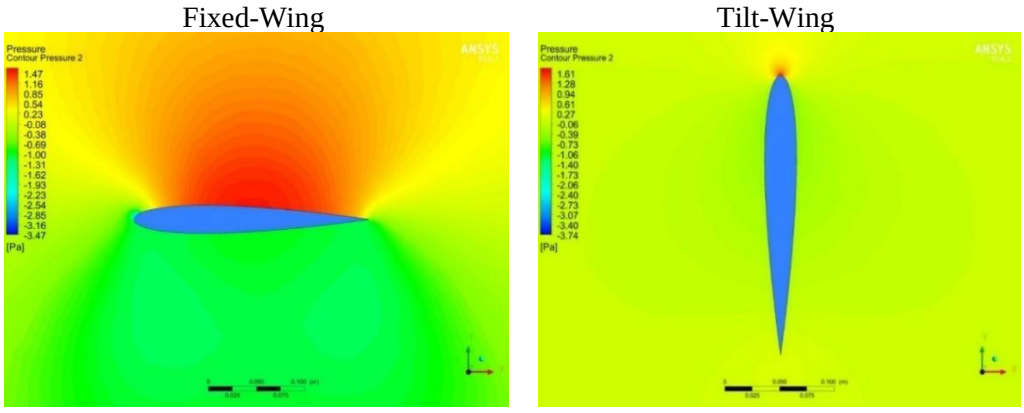

(a)

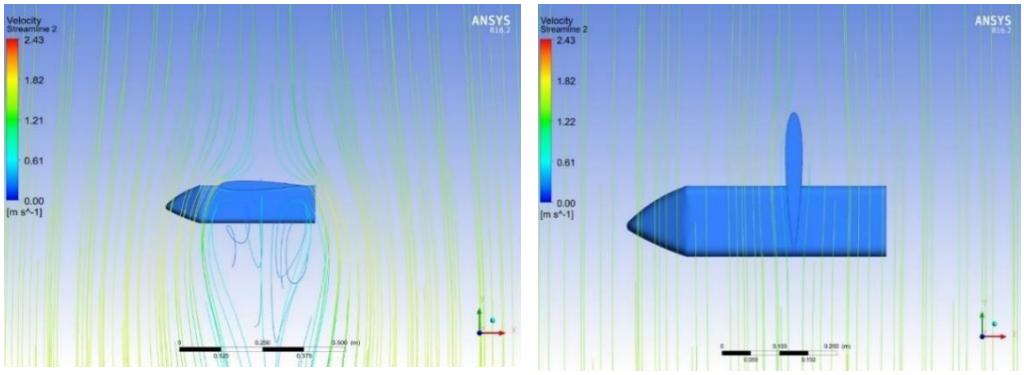

(b)

Figure 4. The results of (a) pressure contour and (b) streamlines at velocity 1.4 m/s

Fixed-Wing Tilt-Wing

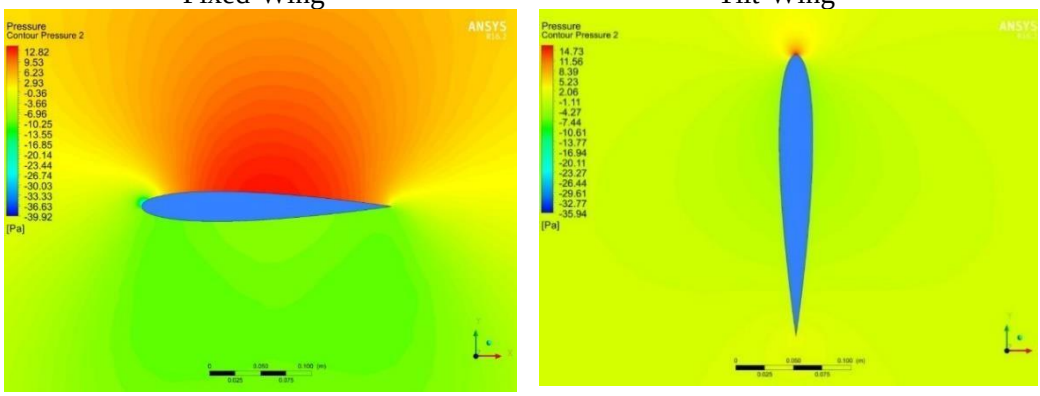

(a)

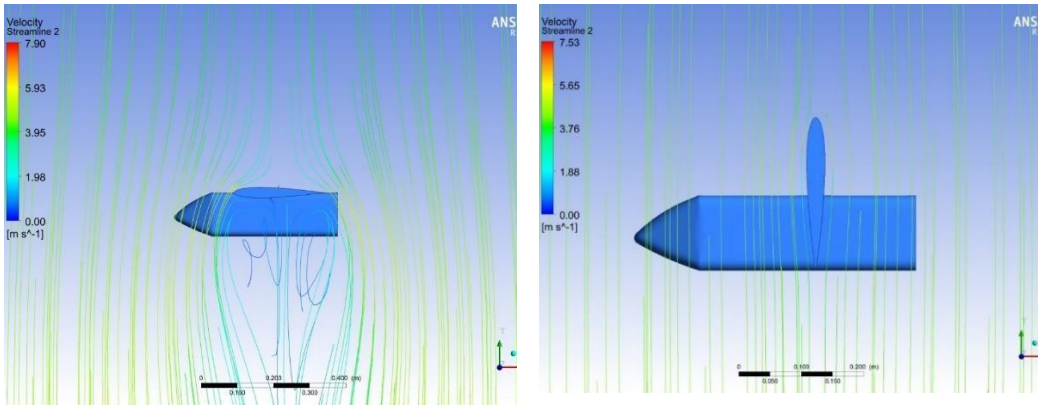

(b)

Figure 5. The results of (a) pressure contour and (b) streamlines at velocity 4.17 m/s

ISSN : 2085-9503 (Print), 2581-1355 (On Line)

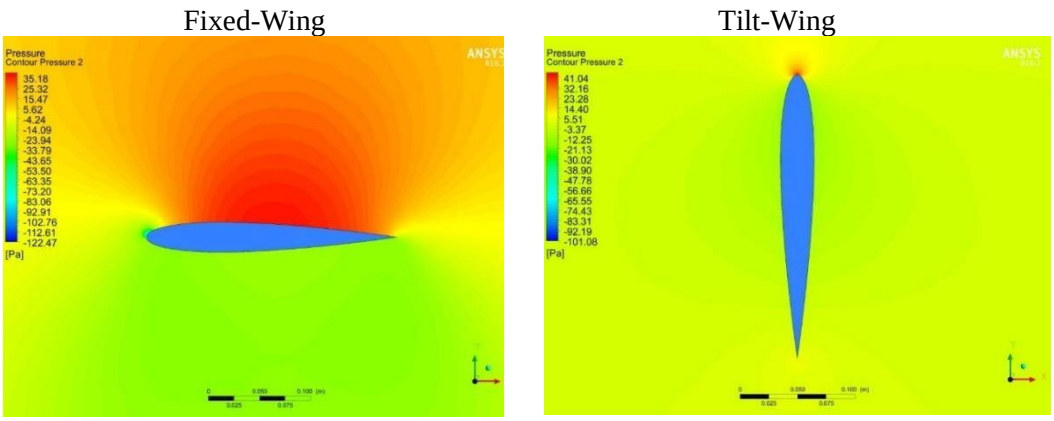

Figure 6. The results of (a) pressure contour and (b) streamlines at velocity 6.94 m/s

The plots of Pressure distribution through the Wing are shown in Figures 7 and 8 for upper and lower Wing, respectively. The black lines denote the Tilt-Wing while the red one was Fixed-Wing. At the top surface, Pressure of Tilt-Wing showed the same trend for cases of A, B, and C, whereby the highest value was obtained at the center of Wing. As the increase of velocities, the values of Pressure were escalated as well. At the center, the values were respectively 1.65Pa, 14.98Pa, and 41.74Pa for A, B, and C. Next, the lowest values were in 0.25c and 0.75c, where c is the chord length. It was obtained the most downward Pressure was -11.52Pa for C variation. On the lower surface, the highest Pressure was 5Pa in C, while the Pressure distribution resembled the upper surface. Meanwhile, the lowest value was found on both leading and trailing edges, which accounted for considerably same at about -10.3Pa. The relatively stable pressure distribution explained that the flow was continuous, as shown in the streamlines result, which contributed to the small drag force.

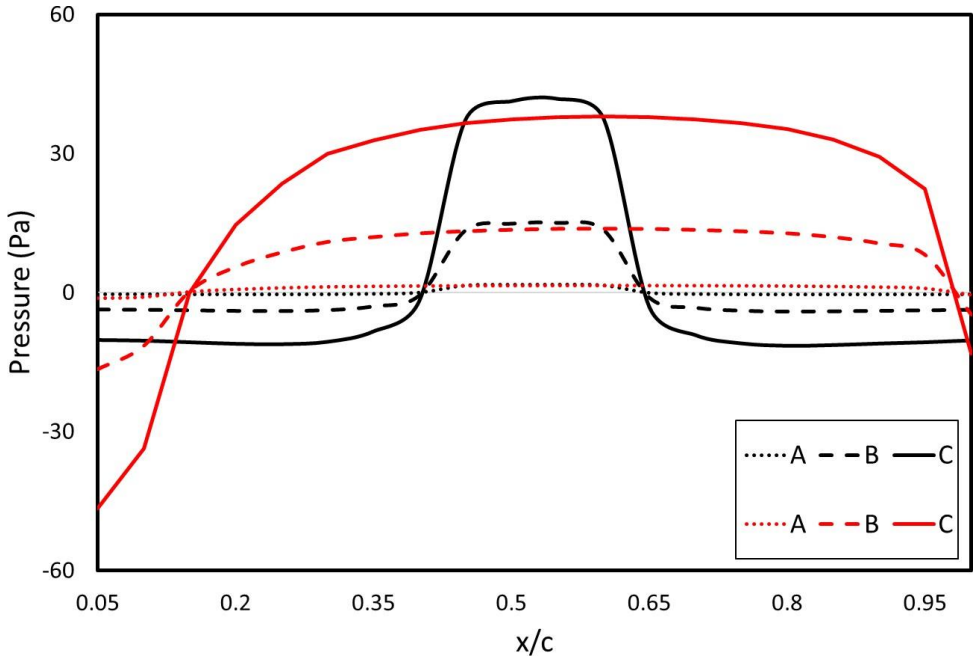

Figure 7. The value of Pressure at upper wing. Black: Tilt-Wing; Red: Fixed-Wing

On the contrary, Fixed-Wing showed different patterns than that of Fixed-Wing. The Pressure was steadily between 0.25c and 0.95c for B and C cases. In the case of A, the Pressure was considerably constant, excluding at 0.05c and 1c. Likewise, on the lower surface, the pressure value was noted in a negative sign that described the direction of negative lift accounted for higher drag. As it can be seen in Figures 7 and 8, the Pressure on the leading and trailing edge significantly decreased, showing the eddy that emerged the turbulence flow. The Pressure distribution described the higher drag value on the Fixed-Wing.

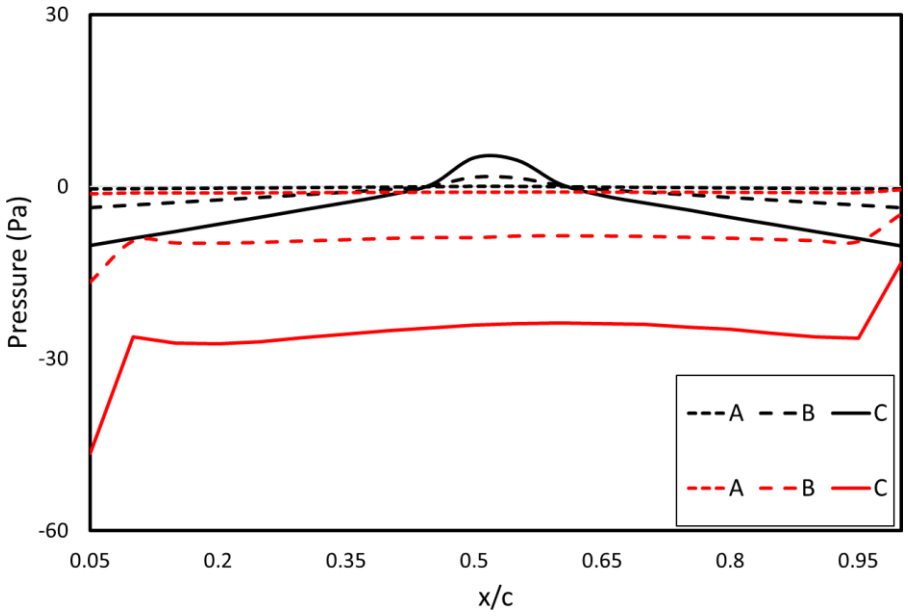

Figure 8. The value of Pressure at lower wing. Black: Tilt-Wing; Red: Fixed-Wing

ISSN : 2085-9503 (Print), 2581-1355 (On Line)

4. CONCLUSION

The simulations of the VTOL UAV are explained in this work. Based on the observed method, the numerical investigation of UAV drag has shown remarkable results. The employed S-A turbulent model has been able to accurately simulate the aerodynamics characteristic of the drag. A parametric study of wind speed was also carried out in order to investigate the optimum performance of the UAV. The drag value of the Hybrid Fixed-Wing UAV aircraft increased from the drag value at a speed of 1.4 m/s to 6.94 m/s. The greatest drag value was at a speed of 6.94 m/s, which was 177.51 N. On the other hand, the drag value of the Tilt-Wing obtained 1.97N at 6.94m/s. This proved that the greater the fluid velocity produced a higher drag value. Moreover, the Pressure distribution on upper and lower surface explained the drag force on both Tilt and Fixed-Wing. This remark led to the power and fuel requirement by fixed-wing UAV aircraft was greater than that of Tilt-Wing UAV aircraft as the higher of drag.

REFERENCES

[1] John F Wendt; John D Anderson, Jr.; Von Karman Institute for Fluid Dynamics.,Computational fluid dynamics : an introduction, Springer, 2008

[2] W.P. Wolfe, S.S. Ochs, "Predicting Aerodynamics Characteristic of Typical Wind Turbine Airfoils Using CFD", Sandia National Laboratories Report

[3] M. R. Ahmed and S. D. Sharma, "An investigation on the aerodynamics of a symmetrical airfoil in ground effect," I., vol. 29, no. 6, pp. 633–647, 2005

[4] Y. Li, J. Wang, and P. Zhang, "Effects of Gurney flaps on a NACA0012 airfoil," Flow, Turbul. Combust. vol. 68, no. 1, pp. 27–39, 2002

[5] S. H. Rhee, S. E. Kim, H. Ahn, J. Oh, and H. Kim, "Analysis of a jet-controlled high-lift hydrofoil with a flap," Ocean Eng., vol. 30, no. 16, pp. 2117–2136, 2003

[6] E. Phillips, R. Woszidlo, and I. Wygnanski, "The dynamics of separation control on a rapidly actuated flap," 5th Flow Control Conf., no. July, pp. 1–16, 2010

[7] N. Rostamzadeh, R. M. Kelso, B. B. Dally, and K. L. Hansen, "The effect of undulating leading-edge modifications on NACA 0021 airfoil characteristics," Phys. Fluids, vol. 25, no. 11, 2013

[8] T. Srinivasa Rao, T. Mahapatra, and S. Chaitanya Mangavelli, "Enhancement of Lift-Drag characteristics of NACA 0012," Mater. Today Proc., vol. 5, no. 2, pp. 5328–5337, 2018

[9] A. Kulshreshtha, S. K. Gupta, and P. Singhal, "FEM/CFD analysis of wings at different angle of attack," Mater. Today Proc., vol. 26, pp. 1638–1643, 2019

[10] Costa Rocha PA, Barbosa Rocha HH, Moura Carneiro FO, Vieira da Silva ME, Valente Bueno A. "kw SST (shear stress transport) turbulence model calibration: a case study on a small scale horizontal axis wind turbine". Energy,2014

[11] Xu He-Yong, Qiao Chen-Liang, Yang Hui-Qiang, Ye Zheng-Yin. "Delayed detached eddy simulation of the wind turbine airfoil S809 for angles of attack up to 90 degrees". Energy 2017.

[12] Sorensen J, Michelsen A, Schreck S. "Navier-Stokes predictions of the NREL phase VI rotor in the NASA Ames 80 ft x 120 ft wind tunnel". Wind Energy 2002.

[13] Dunque PN, Burklund MD, Johnson W. "Navier-Stokes and comprehensive analysis performance predictions of the NREL phase VI experiment". J Sol Energy Eng 2003.

[14] Langtry RB, Gola J, Menter FR. "Predicting 2d airfoil and 3d wind turbine rotor performance using a transition model for general cfd codes", AIAA, vol. 7; 2006

[15] ANSYS Fluent documentation, theory guide, 2016

[16] Spalart PR, Allmaras SR. "A one-equation turbulent model for aerodynamic flows". La Rech Aerospatiale 1994

[17] Andrea C, Valerio D, Francesco B. A, "Spalart-Allmaras turbulence model implementation in a discontinuous Galerkin solver for incompressible flows". J Comput Phys 2013

[18] Haikal, M, M. "Analisis Perbandingan Drag Yang Terjadi Pada Wing Pesawat Uav (Unmanned Aerial Vehicle) Model Tilt Wing Dan Fixed Wing Pada Saat Vtol (Vertical Take Off Landing) Menggunakan Software Cfd (Computational Fluid Dynamics)", Undergraduated thesis, ITDA, 2021

ISSN : 2085-9503 (Print), 2581-1355 (On Line)